Beam Scanning Transmitarray Employing Reconfigurable Dual-Layer Huygens Element

Xuan Wang, Pei-Yuan Qin, *Senior Member, IEEE*, Anh Tuyen Le, *Member, IEEE*, Hao Zhang, Ronghong Jin, *Fellow, IEEE* and Y. Jay Guo, *Fellow, IEEE*

***Abstract*—A Ku-band electronic 2-dimensional (2-D) beam scanning transmitarray employing a new reconfigurable dual-layer Huygens element is developed in this paper. The Huygens element consists of two metallic crosses printed on two layers of a dielectric substrate, respectively, which enables a near non-reflection Huygens resonance. A 1-bit phase compensation with low transmission loss is realized by controlling two PIN diodes on the element. Compared with many other reconfigurable transmitarray elements using multi-layer structures with metallic vias, the proposed reconfigurable Huygens element has a much simpler configuration with a simpler biasing network, and it is not affected by multi-layer alignment errors. This particularly facilitates large aperture array development at higher frequencies. To validate the design concept, an electronically reconfigurable transmitarray with the proposed element is fabricated at 13 GHz. Good agreement between the measured and simulated results is found, showing 2-D scanning beams within ±50° in E plane and ±40° in H plane with a maximum realized gain of 18.4 dBi.**

***Index Terms*—Reconfigurable transmitarray, dual-layer Huygens element, PIN diode, beam scanning.**

I. Introduction

Space-fed arrays, i.e., reflectarrays and transmitarrays, have become more and more attractive since they are able to achieve high gains for many applications, e.g., satellite communications, imaging systems and automotive radars [1]-[4]. The spatial feeding networks employed by reflectarrays [5]-[8] and transmitarrays [9]-[11] have lower loss and cost compared with transmission line based feeding networks employed by phased arrays. The beam scanning of the space-fed arrays can be realized by independently controlling the reflection or transmission phases of the elements on the apertures using PIN didoes, micro-electro-mechanical system (MEMS) switches or varactor didoes. It is worth pointing out that the space-fed arrays have the drawbacks of a high profile and a low efficiency compared with transmission-line-fed phased arrays. Also, reflectarrays have feed blockage issue.

In the last two decades, substantial advances on electronic beam scanning transmitarrays have been developed. A typical method is to use reconfigurable receive-transmit (Rx-Tx) elements printed on different substrate layers [12]-[20]. These elements usually consist of three parts: a receive (Rx) unit, an electronically controlled phase shifter, and a transmit (Tx) unit. In a Rx-Tx element, metallic vias are usually placed to transmit electromagnetic (EM) waves between the Rx and Tx units. Moreover, additional substrate layers are needed for direct current (DC) biasing networks to control the phase shifters. As a result, the configuration of a reconfigurable Rx-Tx element usually contains more than three metallic layers with multiple metallic vias. For example, in [12], [15], and [18], the reconfigurable elements have 4 layers with 18 vias, 6 layers with 7 vias, and 5 layers with 6 vias, respectively.

Another method to achieve beam scanning transmitarrays is to employ frequency-selective surface (FSS) based reconfigurable elements. These elements utilize mutual coupling between multiple metal layers, e.g., three layers in [21], four layers in [22] and five layers in [23], [24] to transmit EM waves through the aperture surfaces without metallic vias. The phase compensation provided by these elements is achieved by varying their resonant frequencies.

According to the above literature review, it can be found that most of the currently reported reconfigurable transmitarray elements have more than three metallic layers with several metallic vias. Such configurations may lead to complex fabrication and package processes, which could affect the performance of transmitarrays. For example, for a 2-bit reconfigurable transmitarray using 6-layer elements with 7 vias at 29 GHz [15], 51 elements were found faulty, which could be due to the fabrication inaccuracies. Hence, it is highly desirable to design dual-layer reconfigurable transmitarray elements without metallic vias, which can also facilitate the design of large-size arrays at higher frequencies.

It should be noted that there are some published dual-layer transmitarray elements using rotated split-ring elements [25], malta-cross elements with metallic vias [26], or patch elements with metallic vias [27]. In those structures, however, the metallic vias increase the element complexity. Furthermore, some dual-layer Huygens elements are reported for transmitarrays [28]-[32]. One particular advantage of Huygens elements is that a near total transmission, zero reflection and full phase coverage can be achieved when the electric and

This work was supported by the Australia Research Council Discovery Program under Grant DP220101158. X. Wang is with the Department of Electronic Engineering, Shanghai Jiao Tong University, Shanghai 200240, China, and also with the Global Big Data Technologies Centre, University of Technology Sydney, Ultimo, NSW 2007, Australia.

P.-Y. Qin, A. T. Le, H. Zhang and Y. J. Guo are with the Global Big Data Technologies Centre, University of Technology Sydney, Ultimo, NSW 2007, Australia (e-mail: pyqin1983@hotmail.com).

R. Jin is with the Department of Electronic Engineering, Shanghai Jiao Tong University, Shanghai 200240, China.

magnetic responses are balanced. This can lead to high efficiency transmitarrays. It should be noted that the above-mentioned dual-layer transmitarray elements are all passive ones and there is no electronic control of their transmission phases. Actually, electronic beam-scanning transmitarrays based on dual-layer reconfigurable elements have been rarely reported.

In this paper, a novel electronic beam scanning transmitarray employing 1-bit reconfigurable dual-layer Huygens element is developed at Ku-band. Two PIN diodes are integrated on the element enabling a near non-reflection Huygens resonance to achieve a 1-bit phase compensation. By employing the proposed element, an electronically reconfigurable transmitarray with a simple biasing network has been designed and fabricated. A measured realized gain of 18.4 dBi and scanning beams within ±50° in E plane and ±40° in H plane are obtained.

The rest of this paper is organized as follows. Section II describes the configurations, working principle, and the frequency responses of the proposed 1-bit reconfigurable dual-layer Huygens element. The design of the reconfigurable transmitarray employing the proposed element is shown in Section III. The simulated and measured results are shown in Section IV. The paper concludes in Section V.

II. Reconfigurable Dual-Layer Huygens Element

A. Dual-Layer Huygens Element

The configuration of the dual-layer Huygens element is demonstrated in Fig. 1. It is composed of two metallic crosses printed on two layers of a dielectric substrate (Rogers RT/duroid 5880, ε_r = 2.2, tanδ = 0.009, h = 3.175 mm). These two metallic crosses are symmetric to x-axis. As advised by the manufactory, the alignment error between the two metal layers on this single substrate is less than 0.1 mm, and simulated results show that this dual-layer Huygens element is insensitive to this alignment error. The lengths of the total metallic strip and the overlapped part of the strips along x-axis on each layer are (a+b) and 2a, respectively. The values of the parameters are as follows: p = 12.24 mm, a = 1.71 mm, b = 6.12 mm, w = 0.49 mm, d = 0.69 mm and l = 2 mm.

The element is simulated using master/slave boundary conditions and Floquet ports of 3D EM software HFSS, considering the loss in the dielectric and using PEC for the metallic parts in the structure. An incident x-polarized plane wave is used to illuminate the element. The simulated transmission and reflection coefficients of the dual-layer Huygens element under the incidence waves with different angles are shown in Fig. 2. It is found that the transmission losses are less than 2.1 dB and the phase variation ranges are 320° from 11 to 15 GHz for the element under the incidence waves with the angles from 0° to 30°. There are two peaks of the transmission magnitudes reaching -0.17 dB at 13.0 GHz and -0.08 dB at 13.8 GHz, respectively. It can also be seen from Fig. 2 that the element has stable transmission performance under the incidence waves with different angles, which is beneficial to a transmitarray design.

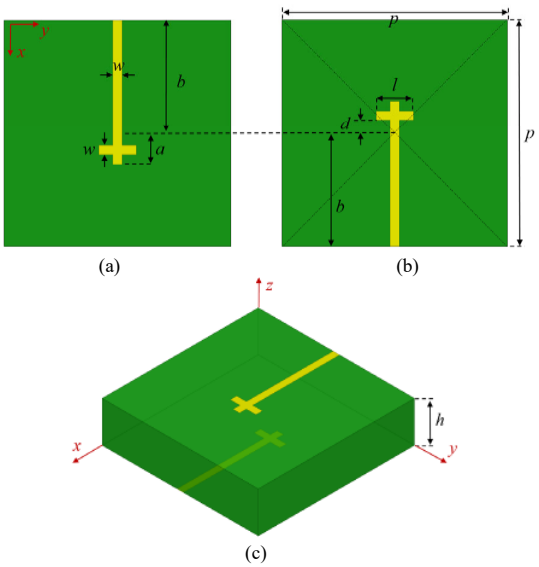

Fig. 1. Configuration of the dual-layer Huygens element. (a) Top view. (b) Bottom view. (c) 3D view.

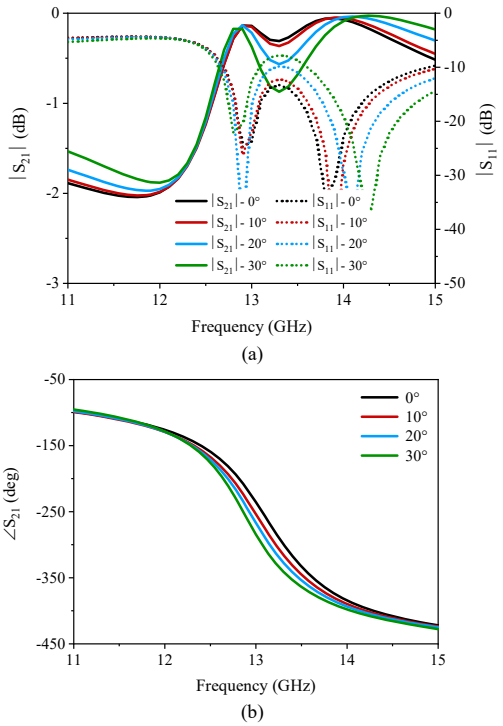

Fig. 2. Transmission and reflection coefficients of the dual-layer Huygens element under the incidence waves with different angles. (a) Magnitudes. (b) Phases.

Based on the Huygens theory, a Huygens resonance can be excited with a total transmission when the orthogonally induced electric and magnetic currents are in-phase [33], [34]. The electric surface admittance (Y_{es}) and magnetic surface impedance (Z_{ms}) can be used to characterize electric and magnetic surface currents. They can be extracted from the reflection and transmission coefficients as follows [35]

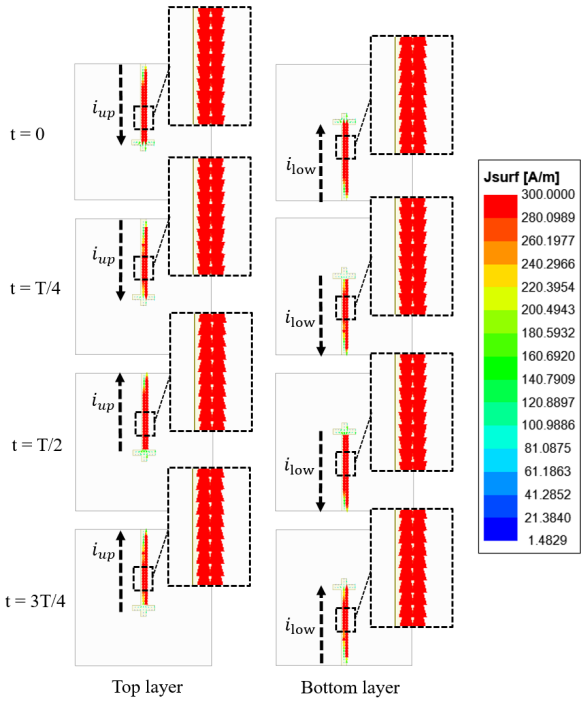

Fig. 3. Simulated current distributions on two layers of the Huygens element.

$$Y_{es} = \frac{2(1-T-R)}{\eta(1+T+R)}, \tag{1a}$$

$$Z_{ms} = \frac{2\eta(1-T+R)}{1+T-R}, \tag{1b}$$

where η is the wave impedance of free space, T is the transmission coefficient and R is the reflection coefficient. It has been demonstrated that a total transmission can be achieved if Y_{es} and Z_{ms} are purely imaginary as given below [35]

$$Y_{es}\eta = \frac{Z_{ms}}{\eta}. \tag{2}$$

The electric and magnetic surface impedances can be calculated using the Z matrix [32]. Therefore, the dimensions of the element can be obtained according to the required surface impedance values.

Based on (1a) and (1b), the simulated $Y_{es}\eta$ and Z_{ms}/η of the dual-layer Huygens element at two transmission peaks are $Y_{es}\eta = 2.87 - j0.03$ and $Z_{ms}/\eta = 1.53 - j0.03$ at 13.0 GHz; $Y_{es}\eta = 0.01 - j1.95$ and $Z_{ms}/\eta = -j1.95$ at 13.8 GHz. It shows that the imaginary parts of $Y_{es}\eta$ and Z_{ms}/η are equal and their real parts are near zero at 13.0 GHz and 13.8 GHz. Thus, at these two frequency points, quasi-Huygens resonances are achieved with very small transmission loss.

When the element is illuminated by an *x*-polarized wave, currents will be induced on the metallic crosses on both layers of the dielectric substrate. The simulated surface currents of the dual-layer Huygens element at 13 GHz are shown in Fig. 3. The currents on top and bottom substrate layers are named as i_{up} and i_{low}, respectively. As shown in Fig. 3, the directions of i_{up} and i_{low} are opposite in the first and third quarters of one time period T, providing a current loop in the overlapped areas of the two strips along *x*-axis on the two layers of the substrate. This current loop can be equivalent to a magnetic current with a time delay of T/4 [34], [35]. In the second and fourth quarters of T, the directions of i_{up} and i_{low} are the same, leading to an electric current. Thus, the orthogonally induced electric and magnetic currents appear simultaneously, exciting a Huygens resonance in the element.

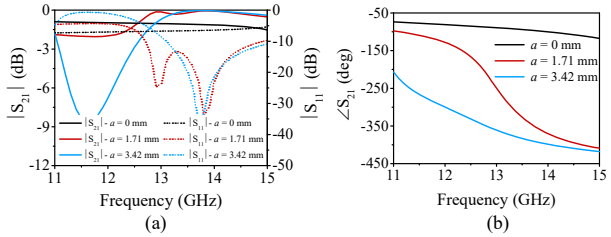

Fig. 4. Transmission and reflection coefficients of the dual-layer Huygens element with different values of parameter *a*. (a) Magnitudes. (b) Phases.

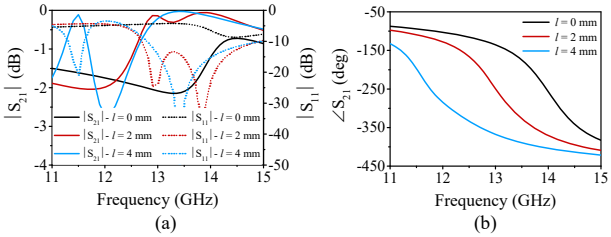

Fig. 5. Transmission and reflection coefficients of the Huygens element with different values of parameter *l*. (a) Magnitudes. (b) Phases.

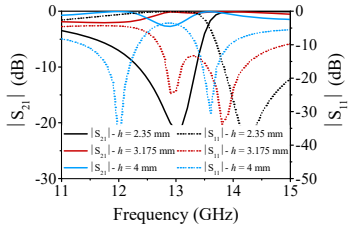

Fig. 6. Transmission and reflection magnitudes of the dual-layer Huygens element with different thickness *h* of the dielectric substrate.

B. Parametric Study

A few parameters are found to play important roles in generating the Huygens resonance. A parametric study is conducted. When one parameter is varied, the others remain stable. The transmission and reflection coefficients of the dual-layer Huygens element with different values of parameter *a* are shown in Fig. 4. It is noticed that the transmission loss and the phase range are dependent by *a*. This means the overlapped part of metallic strips along *x*-axis affects significantly the Huygens resonance. When $a = 0$ (no overlapped part and $l = 0$ mm) or $a = 3.42$ mm (a long overlapped part), the Huygens resonance cannot be excited as the phase coverage is very small or/and the transmission loss is very high in the band. The transmission and reflection coefficients of the element with different values of parameter *l* are shown in Fig. 5. It can be found that the operating frequency and transmission loss of the element are affected by *l*, thus low transmission loss at a desired operating frequency can be achieved by tuning *l*. The transmission and

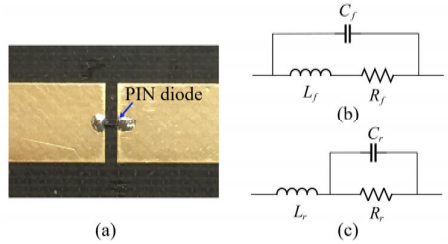

Fig. 7. (a) The PIN diode soldered on a microstrip line. The equivalent circuit models of the PIN diode under (b) forward bias; (c) reverse bias.

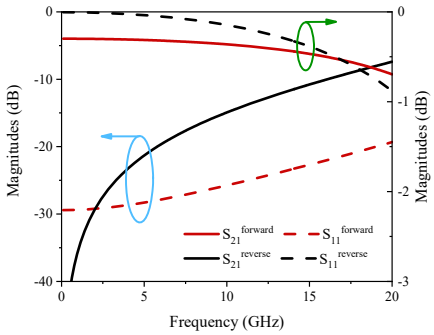

Fig. 8. *S*-parameters of the equivalent circuits of the PIN diode.

reflection magnitudes of the element for different thickness h of the dielectric substrate are shown in Fig. 6. It is seen that the transmission loss of the element is significantly affected by h, which means the thickness of the dielectric substrate affects the Huygens resonance. Overall, the Huygens resonance depends on the induced current loop in relation to two parameters a and h. In this work, the thickness of the element is chosen as 3.175mm as this is a standard thickness for substrate.

C. PIN Diode Experimental Characterization and Modeling

To electronically control the transmission phase of the dual-layer Huygens element, the surface-mount PIN diodes MA4AGP907 fabricated by M/A-Com are employed. A PIN diode MA4AGP907 has been soldered on a microstrip line (The width of the microstrip lines of the fixture is designed to achieve 50 Ohm impedance match.) of a fixture shown in Fig. 7 (a) and measured under forward bias (I_f = 10 mA) and reverse bias (V_r = -5 V) by a vector network analyzer from 100 MHz to 20 GHz. By using the de-embedding method given in [36], the de-embedded results of the diode under forward and reverse biases are obtained. The de-embedded results are fitted to two commonly used equivalent circuit models of a PIN diode as shown in Figs. 7 (b) and 7 (c), and the extracted parameters are as follows: R_f = 3.5 Ω, L_f = 0.055 nH, C_f = 0.42 pF, R_r = 200 kΩ, L_r = 0.66 nH, C_r = 0.027 pF. The *S*-parameters of the extracted equivalent circuit models of the PIN diode from 100 MHz to 20 GHz are shown in Fig. 8.

D. Reconfigurable Dual-Layer Huygens Element

In order to electronically control the beams of a transmitarray for a 2-D beam scanning, the transmission phase of each transmitarray element should be controlled independently. As

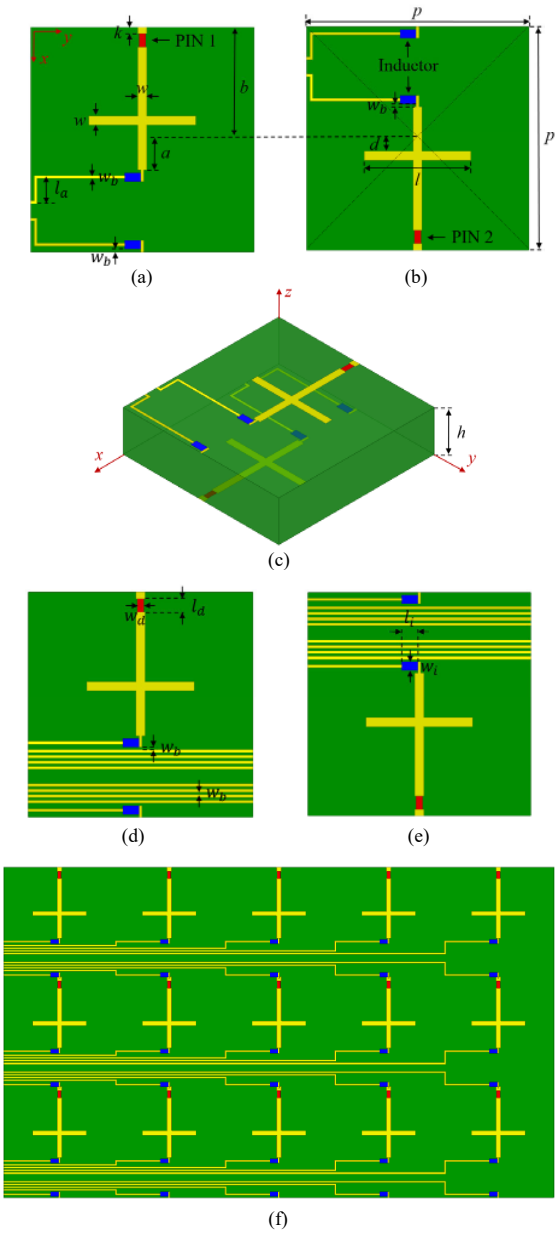

Fig. 9. Configurations of the reconfigurable Huygens elements. (a) Top view; (b) bottom view; (c) 3D view of the element with 4 biasing lines. (d) Top view; (e) bottom view of the element with 20 biasing lines. (f) Top view of a part of the whole transmitarray.

illustrated in Fig. 9, a reconfigurable Huygens element is developed based on the dual-layer Huygens element presented in Section II-A. It is printed on two layers of the same Rogers RT/duroid 5880 dielectric substrate. Two PIN diodes are integrated in these two metallic crosses respectively to achieve 1-bit phase compensation. By using the extracted equivalent circuit models of the PIN diode, the dimensions of the reconfigurable element are changed slightly to achieve 1-bit phase change with a high transmission. The dimensions are as follows: p = 12.24 mm, a = 1.71 mm, b = 6.12 mm, w = 0.49

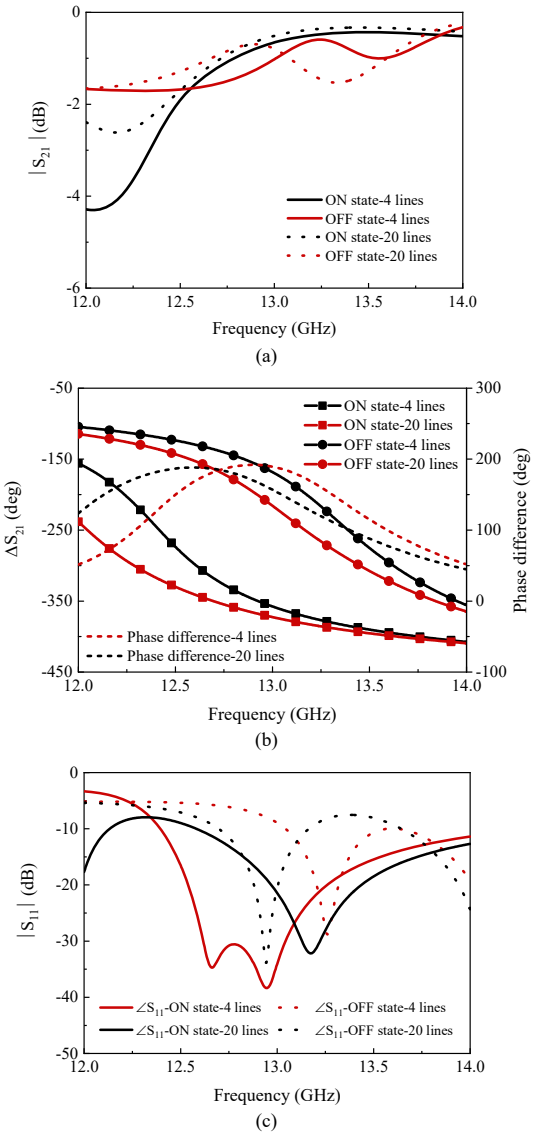

Fig. 10. Transmission and reflection coefficients of the reconfigurable dual-layer Huygens element with 4 or 20 biasing lines under ON and OFF states. (a) Transmission magnitudes. (b) Transmission phases. (c) Reflection magnitudes.

mm, d = 0.77 mm, l = 5.86 mm, k = 0.35 mm, w_b = 0.15 mm, l_a = 1.51 mm, l_d = 0.74 mm, w_d = 0.35 mm, l_i = 0.89 mm, w_i = 0.46 mm. As shown in Figs. 9 (a), 9 (b) and 9 (c), two biasing lines along y-axis are connected to the two ends of the metallic strip along x-axis on each layer of the substrate to control the diodes, and an inductor is embedded in each biasing line to isolate the DC source of the control board from the RF signals. According to the current distributions of the dual-layer Huygens element shown in Fig. 3, these two PIN diodes are located at the places where the currents through the metallic crosses are small. In this way, the extra loss from the PIN didoes can be minimized. These two PIN diodes on the element are switched on or off at the same time. The working states of the element are named as ON or OFF states when these two PIN diodes are under forward or reverse biasing voltages, respectively. For different working states, the resonant lengths of the element are different, leading to different transmission phases. By selecting appropriate parameter k which is the positions of these two diodes, a 1-bit phase shift with a high transmission is achieved between ON and OFF states.

TABLE I
TRANSMISSION MAGNITUDES AND PHASES OF THE RECONFIGURABLE DUAL-LAYER HUYGENS ELEMENT WITH FOUR BIASING LINES AT 13 GHZ

State	PIN 1/PIN 2	Magnitude (dB)	Phase (deg)
ON	ON/ON	-0.65	-353°
OFF	OFF/OFF	-1.02	-173°

By utilizing periodic boundary conditions of the full-wave simulation software CST, the reconfigurable dual-layer Huygens element is simulated. The frequency response of the reconfigurable element with 4 biasing lines is shown in Table I and Fig. 10. It can be seen from Figs. 10 (a) that the transmission loss of the element with 4 biasing lines is lower than 1 dB at 13 GHz. As shown in Fig. 10 (b), the phase difference between ON and OFF states at 13 GHz is 180°, but the phase difference of 180° is only achieved in a narrow band. This is due to the inherent narrow band property of Huygens elements, especially for dual-layer elements. As a result, the array can scan its beam in a narrow band.

When employing the reconfigurable Huygens element to form a transmitarray, different number of biasing lines [Fig. 9 (f)], i.e., 4, 8, 12, 16, 20, will be printed on the elements located at different positions of the transmitarray. In order to evaluate the effects of the biasing lines on frequency responses of the element, the simulation of the reconfigurable elements with 20 biasing lines [Figs. 9 (d) and 9 (e)] under ON and OFF states have been performed as plotted in Fig. 10. It is seen that the transmission phase differences between two states and the transmission magnitudes of the elements with 4 and 20 biasing lines are nearly the same. This is mainly due to the fact that the biasing lines are perpendicular to the electric field polarization. Additionally, the biasing lines are very thin and embedded with inductors.

III. RECONFIGURABLE TRANSMITARRAY ANTENNA

A. Design of Reconfigurable Transmitarray

Limited by the fabrication accuracy, the minimum width of the biasing lines and the space between two biasing lines are both 0.15 mm, which means the proposed reconfigurable Huygens element can be applied to a maximum 12×12 elements beam-scanning transmitarray consisting of two sub-arrays. A larger-size array can be achieved by dividing the array into more sub-arrays for the biasing purpose or re-designing the element's parameters, such as enlarging the element's size or reducing the length of the striplines along the x-axis. In this work, a reconfigurable transmitarray with 10×10 elements is designed. The schematic of the transmitarray prototype with a biasing network and a scanning-control board is shown in Fig. 11, which can be seen as two 10 × 5-element sub-arrays symmetric to x-axis. The size of the transmitarray aperture is

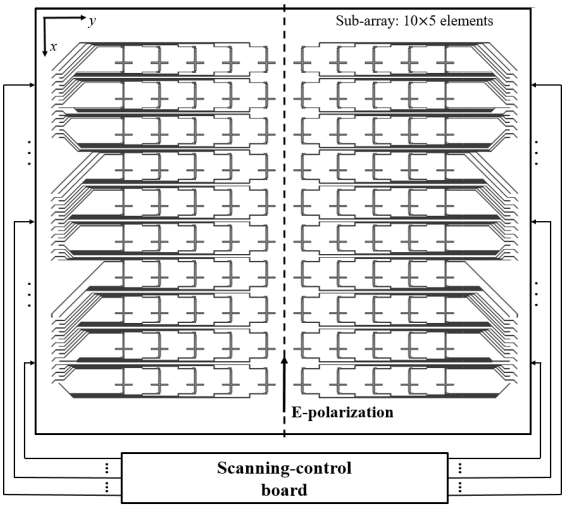

Fig. 11. Schematic of the 10×10 reconfigurable transmitarray with its scanning-control board.

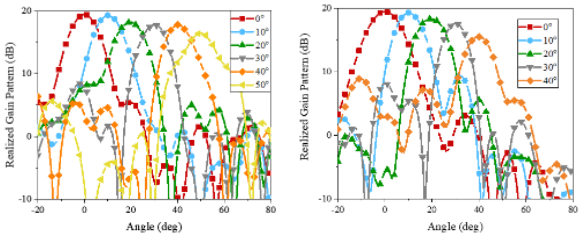

(a) (b)

Fig. 12. Simulated co-polarized radiation patterns at 13 GHz in (a) E plane and (b) H plane.

122 mm × 122 mm. Because the two PIN diodes on any element are switched on or off simultaneously at any given time, the biasing lines of these two PIN diodes can be connected and controlled by one DC source path. Thus, the 10×10-element transmitarray contains 100 independent paths of DC sources to manipulate the transmission phase of each element. These DC bias paths are controlled by a field-programmable gate array (FPGA) based controlling board. Figs. 12 (a) and 12 (b) show the simulated scanning beams of the reconfigurable transmitarray in E plane (*xoz*) and H plane (*yoz*), respectively. It is found that the simulated gain decreases as the scanning angle increases. The scanning loss at 50° is 3.0 dB in E plane and the scanning loss at 40° is 4.0 dB in H plane. The side lobe levels (SLLs) of most scanning beams are larger than 9 dB. Only the SLL of the scanning beam at 40° in H plane is 7 dB. Please note that a larger beam scanning range with lower scanning loss can be achieved if a larger number of bits for the phase compensation is used.

B. Experimental Implementation

The prototype of the 100-element reconfigurable transmitarray fabricated by LINTEK is shown in Fig. 13 (a), which contains 200 PIN diodes and 400 inductors. The experimental implementation is shown in Fig. 13 (b). A

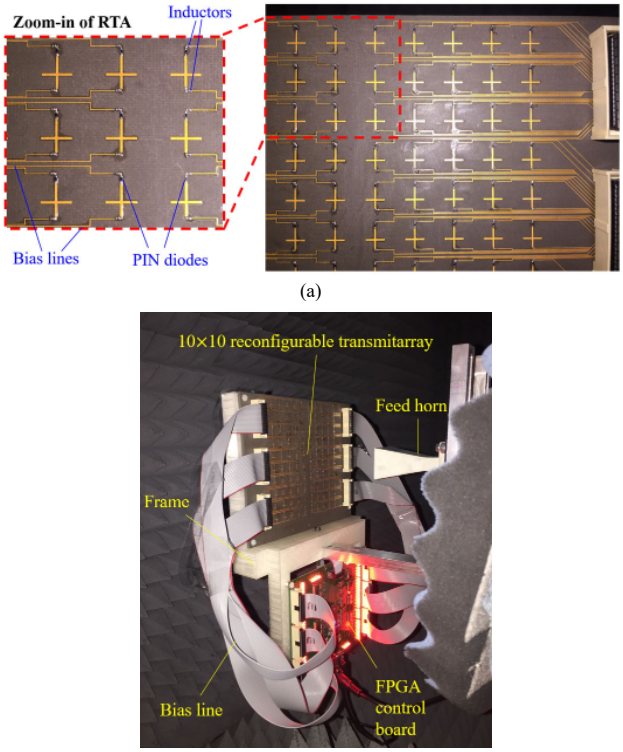

(a) (b)

Fig. 13. Photographs of (a) fabricated reconfigurable transmitarray prototype and (b) experimental implementation of the reconfigurable transmitarray mounted in the anechoic chamber.

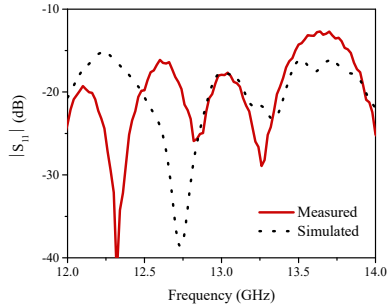

Fig. 14. Measured and simulated input reflection coefficients of the transmitarray radiating towards boresight.

linearly-polarized standard gain horn antenna is placed at the focal point with a -10 dB aperture edge illumination. The focal length is 91 mm, and the F/D ratio is 0.74. The FPGA control board is fixed below the reconfigurable transmitarray by a supporting frame. The FPGA control board contains 100 DC biasing paths with a 10 mA biasing current or -5 V biasing voltage per element. 100 LED lights are connected in series with the 100 DC biasing paths, respectively, in order to show the working status of the transmitarray intuitively. Six insulation-displacement contact (IDC) cables are used to connect the DC power supply from the FPGA control board to the diodes on the transmitarray. By using a digital I/O USB module, the control signals for 2-D beam scanning are provided to the FPGA control board from the computer. The far-field

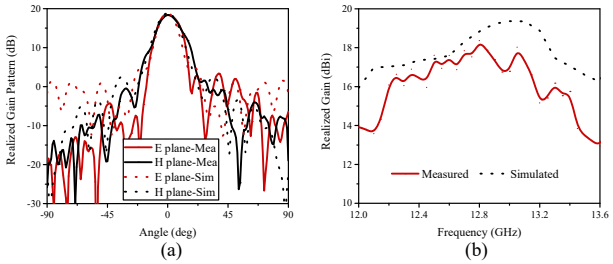

(a) (b)

Fig. 15. (a) Measured and simulated boresight co-polarized radiation patterns in E and H planes at 12.8 GHz. (b) Measured and simulated co-polarized realized gains in boresight direction versus frequencies.

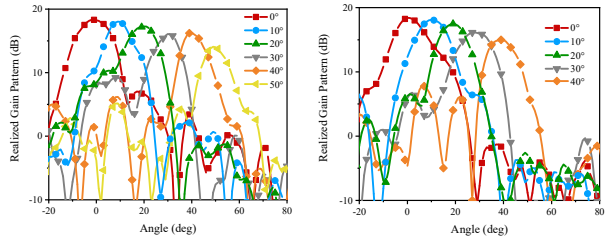

(a) (b)

Fig. 16. Measured co-polarized radiation patterns for different scanning angles at 12.8 GHz in (a) E plane and (b) H plane.

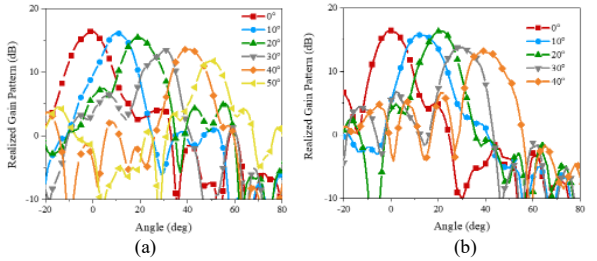

(a) (b)

Fig. 17. Measured co-polarized radiation patterns for different scanning angles at 12.4 GHz in (a) E plane and (b) H plane.

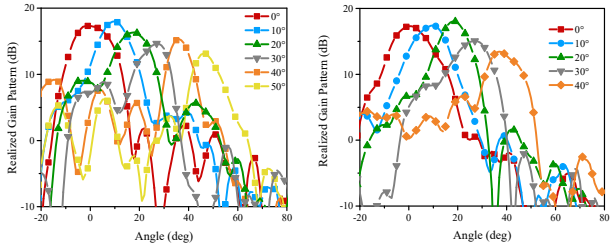

(a) (b)

Fig. 18. Measured co-polarized radiation patterns for different scanning angles at 13.1 GHz in (a) E plane and (b) H plane.

radiation pattens of the transmitarray are measured using a compact range at University of Technology Sydney, Australia.

IV. Numerical and Experimental Results of the Reconfigurable Transmitarray

As shown in Fig. 14, the input reflection coefficients for the boresight radiation pattern of the reconfigurable transmitarray are below -10 dB from 12 GHz to 14 GHz. The input reflection coefficients for other beam scanning angles are also below -10 dB, which are not shown here for brevity. The measured and simulated results on boresight radiation patterns of the transmitarray in E and H planes at 12.8 GHz are shown in Fig. 15 (a) with good agreement. The measured SSL is better than 14 dB in both planes. The measured and simulated realized gains in boresight direction versus frequencies are shown in Fig. 15 (b). The measured maximum realized gain is 18.4 dBi at 12.8 GHz with an aperture efficiency of 20.2 %. The simulated maximum realized gain is 19.5 dBi at 13 GHz. There is a frequency shift of 0.2 GHz and a gain value difference of 1.1 dB. This can be due to the following reasons. Firstly, there could be variations across the properties of the 200 PIN diodes from what we have measured and characterized. Secondly, there could be some fabrication errors during the implementation of the transmitarray and its mounting frame. The measured 3 dB gain bandwidth of the transmitarray is 1.2 GHz from 12.2 GHz to 13.4 GHz, which is 9.4 % at 12.8 GHz.

The measured scanning beams at 12.8 GHz from 0° to 50° in the E plane and from 0° to 40° in the H plane are shown in Figs. 16 (a) and 16 (b), respectively. They are compared with simulated results in terms of the gain values and SLLs, which are shown in Tables II and III for E and H planes, respectively. It is seen that the measured gain decreases as the scanning angle increases. The measured scanning loss at 50° is 4.2 dB in E plane and the measured scanning loss at 40° is 3.4 dB in H plane. The SLLs of most scanning beams are better than 9 dB,

TABLE II
Beam Scanning Performance of the Reconfigurable Transmitarray in E Plane

Scan Angle		0°	10°	20°	30°	40°	50°
Gain (dBi)	Mea.	18.4	18.1	17.4	16.2	16.4	14.2
	Sim.	19.5	19.3	18.3	17.8	17.8	16.5
SLL (dB)	Mea.	11.4	15.9	15.3	7.0	10.2	9.1
	Sim.	14.0	13.2	9.9	9.3	9.5	9.3

TABLE III
Beam Scanning Performance of the Reconfigurable Transmitarray in H Plane

Scan Angle		0°	10°	20°	30°	40°
Gain (dBi)	Mea.	18.4	18.1	17.5	16.1	15.0
	Sim.	19.5	19.3	18.3	17.6	15.5
SLL (dB)	Mea.	19.6	11.9	11.0	9.4	7.3
	Sim.	16.1	9.7	12.2	9.2	7.0

TABLE IV
Gain Loss Analysis for Boresight Beam at 12.8 GHz

Aperture Size	122mm×122mm
Ideal Directivity	25.3 dBi
Spillover Loss	0.2 dB
Taper Illumination Loss	0.5 dB
Phase Quantization Loss	4.0 dB
Reflection Loss and Cross-Polarization Loss	0.1 dB
Element Insertion Loss	1.0 dB
Losses from Fabrication, Alignment, and Measurement Errors	1.1 dB
Measured Gain	18.4 dBi

TABLE V
COMPARISONS BETWEEN THE RECONFIGURABLE TRANSMITARRAY ANTENNAS

Ref.	Theory	Layer No.	Via No.	Diode No.	Frequency	Array size	Gain	Aperture eff.	3-dB gain bandwidth	Measured scanning angle and loss
[9]	Rx-Tx	4	5	2	9.8 GHz	20×20	22.7 dBi	16.0 %	15.8 %	40^o (2.8 dB) × 70^o (7.6 dB)
[12]	Rx-Tx	4	18	2	13.5 GHz	16×16	21.4 dBi	14.7 %	13.3 %	60^o (3.6 dB) × non shown
[13]	Rx-Tx	4	3	2	12.5 GHz	16×16	17.0 dBi	14.0 %	9.6 %	50^o (5.8 dB) × 50^o (5.7 dB)
[15]	Rx-Tx	6	7	4	29.0 GHz	14×14	19.8 dBi	15.9 %	16.2 %	60^o (5.0 dB) × 60^o (5.0 dB)
This work	Huygens	2	None	2	12.8 GHz	10×10	18.4 dBi	20.2 %	9.4 %	50^o (4.2 dB) × 40^o (3.4 dB)

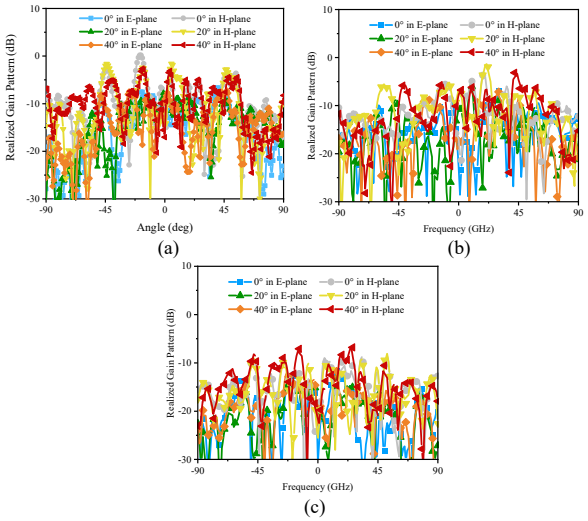

Fig. 19. Measured cross-polarized radiation patterns for different scanning angles in E and H planes. (a) 12.8 GHz. (b) 12.4 GHz. (c) 13.1 GHz.

only the SLLs of the scanning beams at 30° in E plane and 40° in H plane are around 7 dB. The measured scanning beam patterns at 12.4 GHz and 13.1 GHz are shown in Figs. 17 and 18, respectively. At 12.4 and 13.1 GHz, the measured scanning losses at 50° are 4.7 dB and 4.2 dB in E plane, respectively. The scanning losses at 40° are 3.2 dB and 3.9 dB for these two frequency points in H plane, respectively. As shown in Fig. 19, the measured cross-polarized radiation patterns for several scanning angles at 12.4 GHz, 12.8 GHz and 13.1 GHz in E and H planes are all at least 15 dB lower than the co-polarization. The measured cross-polarized gain levels for other scanning angles are also low. They are not shown here for brevity.

Based on the directivity equation $D = 4\pi A/\lambda^2$, where A is the area of the transmitting aperture, the maximum ideal directivity of the boresight beam of the transmitarray is 25.3 dBi. The gain loss is attributed by various factors as summarized in Table IV. The spillover loss and taper illumination loss from the horn antenna are 0.2 dB and 0.5 dB, respectively. Compared with the gain by assuming a continuous phase using array theory, the phase quantization loss of the 1-bit transmitarray is 4.0 dB. The reflection loss and cross-polarization loss of the transmitarray are 0.1 dB, which can be obtained by full-wave simulation. The element insertion loss is estimated to be 1.0 dB, which is the average value of ON and OFF states with different incident angles. By comparing the measured and simulated results of the beam scanning transmitarray, the losses from the fabrication, alignment, and measurement errors are 1.1 dB.

A compaison between other reconfigurable transmitarrays and the developed one is presented in Table V. It can be found that the proposed work employs much simpler array elements, i.e., dual-layer Huygens configuration without any metallic vias. As a comparison, the other array elements have at least four metallic layers and many vias. Although the structure of the proposed element is simpler, the performance of the transmitarray is comparable to those of other arrays. The proposed dual-layer reconfigurable Huygens element without metallic vias is particular suitable for larger-size beam scanning transmitarrays at higher frequency bands. The largest beam scanning angles of the array are mainly affected by the phase compensation errors. This can be addressed by using either 2-bit phase compensation or smaller array elements. However, these two methods will increase the design complexity. Consequently, compromise should be made between the design complexity and scanning angles for beam scanning transmitarrays.

V. CONCLUSION

A novel electronic beam scanning transmitarray employing dual-layer reconfigurable Huygens element is reported in this paper. The Huygens element is composed of two metallic crosses which enables a near non-reflection response. Moreover, the element can achieve a 1-bit phase compensation with low transmission loss by controlling two PIN diodes on the element. A reconfigurable transmitarray with a simple biasing network is designed and fabricated for the experimental verification. The measured maximum gain in the boresight direction is 18.4 dBi with an aperture efficiency of 20.2 %, and the 3-dB gain bandwidth is 9.4 %. The 2-D electronic beam scanning of ±50° in E plane and ±40° in H plane is achieved.

REFERENCES

[1] S. B. Yeap, X. Qing, and Z. N. Chen, "77-GHz dual-layer transmit-array for automotive radar applications," *IEEE Trans. Antennas Propag.*, vol. 63, no. 6, pp. 2833-2837, Jun. 2015.
[2] Q. Luo, S. Gao, W. Liu, C. Gu, "Low-cost smart antennas," John Wiley & sons, March 2019.
[3] L. Dussopt, "Transmitarray antennas", in A. Boriskin and R. Sauleau (eds), Aperture Antennas for millimeter and sub-millimeter wave applicatons, Springer 2018.
[4] S. V. Hum and J. Perruisseau-Carrier, "Reconfigurable reflectarrays and array lenses for dynamic antenna beam control: A review," *IEEE Trans. Antennas Propag.*, vol. 62, no. 1, pp. 183--198, Jan. 2014.

[5] J. Han, L. Li, G. Liu, Z. Wu and Y. Shi, "A Wideband 1 bit 12 × 12 Reconfigurable Beam-Scanning Reflectarray: Design, Fabrication, and Measurement," in *IEEE Antennas Wireless Propag. Lett.*, vol. 18, no. 6, pp. 1268-1272, June 2019.

[6] Z. Wang et al., "1 Bit Electronically Reconfigurable Folded Reflectarray Antenna Based on p-i-n Diodes for Wide-Angle Beam-Scanning Applications," in *IEEE Trans. Antennas Propag.*, vol. 68, no. 9, pp. 6806-6810, Sept. 2020.

[7] H. Yang et al., "A 1-Bit 10×10 Reconfigurable Reflectarray Antenna: Design, Optimization, and Experiment," in *IEEE Trans. Antennas Propag.*, vol. 64, no. 6, pp. 2246-2254, June 2016.

[8] F. Wu, R. Lu, J. Wang, Z. H. Jiang, W. Hong and K. -M. Luk, "A Circularly Polarized 1 Bit Electronically Reconfigurable Reflectarray Based on Electromagnetic Element Rotation," in *IEEE Trans. Antennas Propag.*, vol. 69, no. 9, pp. 5585-5595, Sept. 2021.

[9] A. Clemente, L. Dussopt, R. Sauleau, P. Potier, and P. Pouliguen, "Wideband 400-Element Electronically Reconfigurable Transmitarray in X Band", *IEEE Trans. Antennas Propag.*, Vol. 61, No. 10, October 2013.

[10] J. G. Nicholls and S. V. Hum, "Full-Space Electronic Beam-Steering Transmitarray With Integrated Leaky-Wave Feed," in *IEEE Trans. Antennas Propag.*, vol. 64, no. 8, pp. 3410-3422, Aug. 2016.

[11] S. Qu, H. Yi, B. J. Chen, K. B. Ng and C. H. Chan, "Terahertz Reflecting and Transmitting Metasurfaces," in *Proc. IEEE*, vol. 105, no. 6, pp. 1166-1184, June 2017.

[12] Y. Wang, S. Xu, F. Yang and M. Li, "A Novel 1 Bit Wide-Angle Beam Scanning Reconfigurable Transmitarray Antenna Using an Equivalent Magnetic Dipole Element," in *IEEE Trans. Antennas Propag.*, vol. 68, no. 7, pp. 5691-5695, July 2020.

[13] M. Wang, S. Xu, F. Yang, and M. Li, "Design and Measurement of a 1-bit Reconfigurable Transmitarray With Subwavelength H-Shaped Coupling Slot Elements", *IEEE Trans. Antennas Propag.*, Vol. 67, No. 5, May 2019.

[14] Y. Xiao, F. Yang, S. Xu, M. Li, K. Zhu and H. Sun, "Design and Implementation of a Wideband 1-Bit Transmitarray Based on a Yagi–Vivaldi Unit Cell," in *IEEE Trans. Antennas Propag.*, vol. 69, no. 7, pp. 4229-4234, July 2021.

[15] F. Diaby, A. Clemente, R. Sauleau, K. T. Pham and L. Dussopt, "2 Bit Reconfigurable Unit-Cell and Electronically Steerable Transmitarray at Ka-Band," in *IEEE Trans. Antennas Propag.*, vol. 68, no. 6, pp. 5003-5008, June 2020.

[16] C. Cheng, B. Lakshminarayanan and A. Abbaspour-Tamijani, "A Programmable Lens-Array Antenna With Monolithically Integrated MEMS Switches," in *IEEE Trans. Microw. Theory Techn.*, vol. 57, no. 8, pp. 1874-1884, Aug. 2009.

[17] C. Cheng and A. Abbaspour-Tamijani, "Study of 2-bit Antenna–Filter–Antenna Elements for Reconfigurable Millimeter-Wave Lens Arrays," in *IEEE Trans. Microw. Theory Techn.*, vol. 54, no. 12, pp. 4498-4506, Dec. 2006.

[18] C. Huang, W. Pan and X. Luo, "Low-Loss Circularly Polarized Transmitarray for Beam Steering Application," in *IEEE Trans. Antennas Propag.*, vol. 64, no. 10, pp. 4471-4476, Oct. 2016.

[19] J. Y. Lau, and S. V. Hum, and M. Li, "Reconfigurable Transmitarray Design Approaches for Beamforming Applications", *IEEE Trans. Antennas Propag.*, Vol. 60, No. 12, December 2012.

[20] F. Wu, J. Wang, R. Lu, X. Xia, W. Hong and K.-M. Luk, "Wideband and low cross-polarization transmitarray using 1 bit magnetoelectric dipole elements," *IEEE Trans. Antennas Propag.*, vol. 69, no. 5, pp. 2605-2614, May 2021.

[21] O. Koutsos, F. F. Manzillo, A. Clemente and R. Sauleau, "Analysis, Rigorous Design and Characterization of a Three-layer Anisotropic Transmitarray at 300 GHz," in *IEEE Trans. Antennas Propag.*, doi: 10.1109/TAP.2022.3145506.

[22] B. D. Nguyen, C. Pichot, "Unit-Cell Loaded With PIN Diodes for 1-Bit Linearly Polarized Reconfigurable Transmitarrays", *IEEE Antennas Wireless Propag. Lett.*, Vol. 18, No. 1, January 2019.

[23] L. Boccia, I. Russo, G. Amendola, G. D. Massa, "Multilayer antenna-filter antenna for beam-steering transmit-array applications," *IEEE Trans. Antennas Propag.,* vol. 60, no. 7, pp. 2287–2300, Jul. 2012.

[24] J. R. Reis, R.F.S. Caldeirinha, A. Hammoudeh, and N. Copner, "Electronically Reconfigurable FSS-Inspired Transmitarray for 2-D Beamsteering", *IEEE Trans. Antennas Propag.*, Vol. 65, No. 9, September 2017.

[25] X. Zhang, F. Yang, S. Xu, A. Aziz, and M. Li, ''Dual-layer transmitarray antenna with high transmission efficiency,'' *IEEE Trans. Antennas Propag.*, vol. 68, no. 8, pp. 6003–6012, Aug. 2020.

[26] W. An, S. Xu, F. Yang, and M. Li, "A double-layer transmitarray antenna using melta crosses with vias," *IEEE Trans. Antennas Propag*., vol. 64, no. 3, pp. 1120–1125, Mar. 2016.

[27] X. Yi, T. Su, X. Li, B. Wu, and L. Yang, "A double-layer wideband transmitarray antenna using two degrees of freedom elements around 20 GHz," *IEEE Trans. Antennas Propag*., vol. 67, no. 4, pp. 2798–2802, Apr. 2019.

[28] L. W. Wu, H. F. Ma, Y. Gou, R. Y. Wu, Z. X. Wang, M. Wang, X. Gao, and T. J. Cui, "High-transmission ultrathin Huygens' metasurface with 360 phase control by using double-layer transmitarray elements," *Phys. Rev. Appl.* 12(2), 024012 (2019).

[29] C. Xue, J. Sun, L. Niu and Q. Lou, "Ultrathin Dual-Polarized Huygens' Metasurface: Design and Application." *Annalen der Physik* 532.7 (2020): 2000151.

[30] M. R. Akram, C. He, and W. Zhu, "Bi-layer metasurface based on Huygens' principle for high gain antenna applica-tions." *Opt. Express* 28.11 (2020): 15844-15854.

[31] C. Xue, Q. Lou, and Z. N. Chen, "Broadband double-layered Huygens' metasurface lens antenna for 5G millimeter-wave systems," *IEEE Trans. Antennas Propagat.*, vol. 68, no. 3, pp. 1468–1476, 2020.

[32] L. -Z. Song, P. -Y. Qin and Y. J. Guo, "A High-Efficiency Conformal Transmitarray Antenna Employing Dual-Layer Ultrathin Huygens Element," in *IEEE Trans. Antennas Propagat.*, vol. 69, no. 2, pp. 848-858, Feb. 2021.

[33] F. Wu, J. Wang, R. Lu, X. Xia, W. Hong and K. -M. Luk, "Wideband and Low Cross-Polarization Transmitarray Using 1 Bit Magnetoelectric Dipole Elements," in *IEEE Trans. Antennas Propagat.*, vol. 69, no. 5, pp. 2605-2614, May 2021.

[34] W. Lin, R. W. Ziolkowski, J. Huang, "Electrically Small, Low-Profile, Highly Efficient, Huygens Dipole Rectennas for Wirelessly Powering Internet-of-Things Devices," *IEEE Trans. Antennas Propag.,* vol. 67, no. 6, pp. 3670-3679, Mar. 2019.

[35] C. Pfeiffer and A. Grbic, "Metamaterial Huygens' surfaces: Tailoring wave fronts with reflectionless sheets," *Phys. Rev. Lett.*, vol. 110, no. 19, pp. 197401, May 2013.

[36] W. Wang, R. Jin, T. S. Bird, H. Fan, X. Liang and J. Geng, "A Multifixture Full-Wave De-Embedding Method for Characterizing One-Port Devices," in *IEEE Trans. Microw. Theory Tech.*, vol. 64, no. 11, pp. 3894–3910, Nov. 2016.